

Switching Effects in Molecular Electronic Devices

Zihao Liu¹ · Shizhao Ren¹ · Xuefeng Guo¹

Received: 9 November 2016 / Accepted: 25 April 2017 / Published online: 10 May 2017
© Springer International Publishing Switzerland 2017

Abstract The creation of molecular electronic switches by using smart molecules is of great importance to the field of molecular electronics. This requires a fundamental understanding of the intrinsic electron transport mechanisms, which depend on several factors including the charge transport pathway, the molecule–electrode coupling strength, the energy of the molecular frontier orbitals, and the electron spin state. On the basis of significant progresses achieved in both experiments and theory over the past decade, in this review article we focus on new insights into the design and fabrication of different molecular switches and the corresponding switching effects, which is crucial to the development of molecular electronics. We summarize the strategies developed for single-molecule device fabrication and the mechanism of these switching effects. These analyses should be valuable for deeply understanding the switching effects in molecular electronic devices.

Keywords Molecular electronics · Device fabrication · Switching effects

This article is part of the Topical Collection “Molecular-Scale Electronics: Current Status and Perspective”; edited by Xuefeng Guo.

Zihao Liu and Shizhao Ren contributed equally to this work.

✉ Xuefeng Guo
guoxf@pku.edu.cn

¹ Beijing National Laboratory for Molecular Sciences, State Key Laboratory for Structural Chemistry of Unstable and Stable Species, College of Chemistry and Molecular Engineering, Peking University, Beijing 100871, People’s Republic of China

1 Introduction

With the aspiration of miniaturization of silicon-based integrated circuit, using single molecules to build functional devices seems to be a promising alternative solution for this issue. To this end, molecular switches, rectifiers, and transistors have been extensively studied in the past decades [1]. Among these devices, molecular switches have attracted great attention because switches are basic components of most electronic devices with broad applications in information storage, logic data manipulation, and signal processing.

In electrical engineering, a switch is an electrical component that can break an electrical circuit, interrupting the current or diverting it from one conductor to another. The mechanism of a macro-size switch may be operated directly by a human operator to control a circuit, may be operated by a moving object such as a door-operated switch, or may be operated by some sensing element for pressure, temperature, or flow. In contrast, the fabrication of molecular switches is entirely different. Firstly, a molecular material with reliable switching should be properly designed. The switching molecule should have reversible bistable states that might possess different electron conductance. An anchoring group is needed for integrating the functional molecule into an electrical circuit. For potential applications in the field of logic gates and memory storage, the on/off ratio of the switch should be large enough to be distinguished. These electrical switches based on single molecules have obvious advantages such as size (several nanometers), speed (potential switching times ~ 100 ps), and stability. Secondly, the technique capable of linking a single molecule into the circuit should be developed [2].

A wide variety of triggers, including physical ones, such as light [3–17], mechanical stimulation [18], bias voltage [19], and temperature, and chemical ones, such as electrochemical gate [20], pH [21], and chemical reactant [22], have been used to tune the molecular electron transport property. Accordingly, on the basis of the switching mechanisms, the devices can typically be divided into two types: conformation-induced and charging/redox switches [2]. In the first case, a molecular isomerization will happen, which is caused by chemical bond formation and cleavage. In the second case, the molecule takes up (or gives up) an electron, leading to a charge state alteration. In some conditions, the molecular behavior cannot be observed directly. Theoretical computation is always used to explain the mechanism of the experimental results and guide the design of molecular switches.

In this review, we start with the introduction of the fabrication of single-molecule junctions. Then we overview the principles used for building a single-molecule switch. Finally, we review another kind of switch based on molecular monolayers. This research field is a quickly growing one. Having limited reference and space, we will only be able to cover some major contributions and highlight some important points. Readers who feel interested can read several superior review articles covering the different aspects of molecular switches [1, 2, 23].

2 Single-Molecule Device Fabrication

One of the biggest challenges in molecular electronics is to develop reliable strategies for building robust molecular junctions at the molecular level. In this regard, discrete methods have been developed and can be classified into two main methods: one is based on metal electrodes and the other is based on carbon electrodes. Metal electrode fabrication strategies include scanning tunneling microscopy break junction (STM-BJ), mechanically controllable break junction (MCPBJ), electro-migration break junction, electrochemical deposition junction, surface-diffusion-mediate deposition junction. Carbon electrodes are usually fabricated by carbon nanotubes and graphene. There is a particular review elsewhere [1]. Here, we briefly introduce the frequently used methods for building single-molecule electronic switches including STM-BJ, MCPBJ, and carbon electrode fabrication.

2.1 Molecular Junction Based on Metal Electrodes

2.1.1 Scanning Tunneling Microscopy Break Junction (STM-BJ)

Scanning tunneling microscopy (STM) has played an important role and been widely used in the field of molecular electronics. Molecules are linked between a metal tip and a conductance substrate by forming covalent bonds between the molecules and the electrodes. Typically, the molecules have an opportunity to bridge both the tip and the substrate when pulling the tip close enough to the substrate. During pulling away the tip from the substrate, the number of bridged molecule can be changed. Finally, the metal–molecular–metal junction is broken. As a STM-BJ is highly reproducible, tens of thousands of molecular conductance curves can be obtained in a test. Through statistical analysis, the random error of a single test can be reduced (Fig. 1).

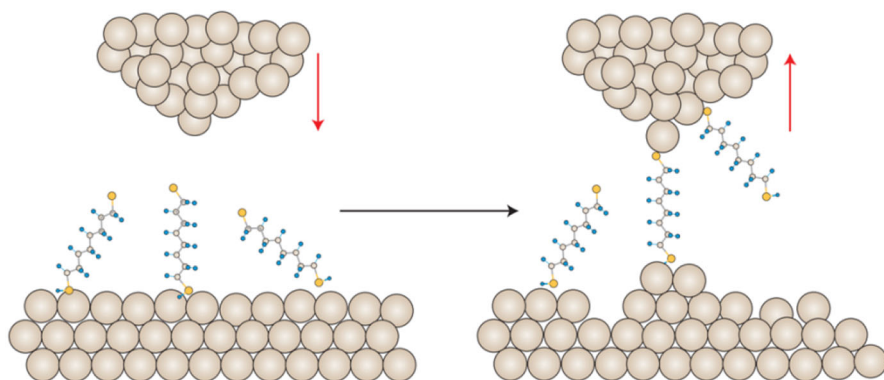


Fig. 1 STM break junction technique used to form single Au-molecule–Au junctions. When the Au tip moves into the Au substrates, which are covered with target molecules, molecule junctions are formed. As the Au tip is lifted, the molecular bridges then lose contact with either the tip or the Au substrate. Reproduced with permission from Ref. [24]. Copyright 2005 Nature Publishing Group

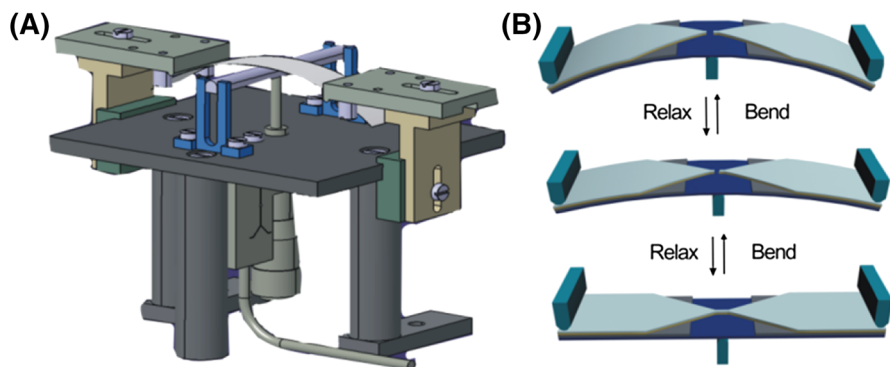


Fig. 2 **a** A schematic of the MCBJ setup. **b** The working principle of the MCBJ setup. A suspended metal bridge with a constriction is microfabricated onto the substrate. When the push rod adds a bending force on the substrate, the movement in the Z direction causes an elongation of the constriction until a break occurs in the metal bridge, resulting in the formation of two separated nanoscale electrodes. Reproduced with permission from Ref. [25]. Copyright 2013 Wiley-VCH

2.1.2 Mechanically Controllable Break Junction (MCBJ)

Mechanically controllable break junction represents a fundamental technique for investigating molecular electronic junctions, especially for the study of the electronic properties of single molecules [25]. The MCBJ technique offers a continuously tunable gap size between two tip-shaped electrodes with the impressive mechanical stability for building a single-molecule device. An MCBJ setup typically consists of three parts: a flexible substrate containing a macrofabricated metal wire or patterned nanostructure, a push rod to break the nanostructure, and a counter support to bend the substrate. A vertical movement of the push rod, which can be accurately controlled by a piezoelectric actuator or motor, can exert a force on the bending beam. As the beam is bent, the metal wire starts to elongate and this leads to the reduction of the cross section at the notch and finally leads to a break of the metal wire (Fig. 2).

The MCBJ technique has several advantages. (1) The MCBJ setup can be easily integrated with other systems such as high vacuum system or Raman spectrometer. (2) A fresh break cross section of the gold bridge is mechanically created by the MCBJ experiment without additional chemical treatments. The pollutant is depressed in the fresh electrodes. (3) The disturbing effect from the push rod can be strongly reduced on the junction. Because of mechanical configuration of the three-point bend apparatus, the vertical motion of the push rod (ΔX) causes only a highly reduced horizontal displacement (ΔZ) of the electrodes ($\Delta Z/\Delta X > 10,000$). (4) Benefited from lithographic techniques, the electrode can be scaled down to molecular dimension, which is suitable for single-molecule measurements. Furthermore, the bridged molecular number can be precisely changed by controlling the gap size.

2.2 Carbon-Based Molecular Junction

Since their discovery of carbon nanotubes in 1991 [26] and graphene in 2004 [27], carbon materials, which mean the allotropes of carbon, have been drawing more and more attention because of their unique features. On the other hand, with the development of nanoscale devices, the scale of electrical devices has been decreased to the nanoscale, resulting in numerous problems in silicon-based devices [28]. One possible way to overcome these difficulties is to find other suitable materials to replace silicon. Carbon materials are the most promising one. Single-walled carbon nanotubes (SWCNTs) [29–33] and graphene [34] are typical ones.

SWCNTs and graphene are made of carbon atoms, which are hybridized with other three atoms, forming a network of sp^2 -hybridized carbon atoms. Carbon is the most basis element in creatures, making SWCNTs and graphene compatible to bio/organic molecules [35, 36]. Compared with metal electrodes, SWCNTs and graphene have a more clear and robust connection with molecules [37], making the experimental results more reproducible [38]. In combination with the ability of mass producing SWCNTs and graphene, all these features make them excellent electrodes for single-molecule devices [1, 39].

There are two key elements in fabricating a single-molecule device with carbon electrodes [1, 37, 38]. The first one is the formation of nanoscale gaps, which must be suitable for unique molecules with the controllable size and the defined edge structure. A proper gap size affords a high yield of device fabrication, and the clear structure offers the experimental data with a small variation. As for SWCNTs [1], the mostly used approaches for gap formation are focused-ion-beam etching, electrical breakdown, and lithography-defined oxidative cutting. Electrical burning [40] and dash-line lithography [34] are the most used ways for gap formation on graphene. The other key element is the way to link molecules. Different connection methods result in different interfaces between molecules and electrodes, which affect the conducting ability effectively. One approach is to bond the electrodes and molecules covalently through chemical reactions. The other one is physical absorption such as π - π stacking, using aromatic rings as the anchoring groups.

2.2.1 SWCNTs

SWCNTs were discovered earlier than graphene, having a more detailed study in single-molecule devices [36]. SWCNT is a one-dimensional nanowire with the configuration-dependent conductance [37], which makes the contribution to the electrical versatility. Every atom of SWCNTs is exposed to an external environment, making them highly sensitive to external stimuli. It is easy to be decorated with functional groups, which can be covalently bonded with molecules in a robust way. The low-dimensional nature can produce nanoscale gaps that are comparable with the molecule's size. These advantages make SWCNTs extraordinary electrodes in single-molecule devices.

In 2006, Guo et al. [41] constructed a covalently bonded single-molecule device based on SWCNT electrodes. They used a lithography-defined oxidative cutting method to form gaps with carboxyl ends. Firstly, SWCNT was spanned with PMMA, then electron beam lithography (EBL) was used to form a window

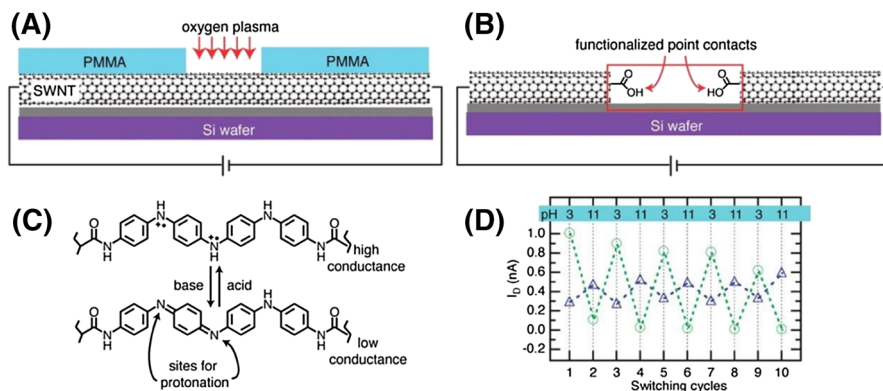


Fig. 3 **a** Etching SWCNTs with oxygen plasma induced through a window of PMMA formed by e-beam lithography. **b** Two SWCNT electrodes with carboxylic acids on the end. **c** Oligoanilines show low/high conductance with the protonation and deprotonations process. **d** Green circles show the pH dependence of oligoanilines. The blue triangles show a slight change of conductance in control groups. Reproduced with permission from Ref. [41]. Copyright 2006 AAAS

precursor of less than 10 nm in PMMA (Fig. 3a), followed by using reactive ion etching (RIE) to etch away the exposed SWCNTs, thus forming a gap between SWCNTs with carboxyl groups on both ends (Fig. 3b). Functional molecules with amino terminals can covalently bond with SWCNT electrodes through amination reactions. The diameter of SWCNTs limits the number of molecules connected in the gap, making it a real single-molecule device. More importantly, covalent bonds offer the devices great robustness and reliability, ensuring that the device can undergo extreme conditions. They had several molecules with different functions bonded with carbon electrodes. Among them, oligoanilines (Fig. 3c) showed low/high conductance corresponding to the inherent protonation and deprotonations processes. The high/low conductance of molecules resulted in the on/off states of the devices, which can be proven by the fluctuation of currents through the devices. When the devices were immersed in solution with different pH in turn, correspondingly the current showed an alternate switch (Fig. 3d), thus affording an ultrasensitive pH sensor. Moreover, with the diversity of the molecular structures, the devices can be fabricated with other desired functionalities.

As the electrodes of single-molecule devices, SWCNTs exhibit good compatibility with numerous functional molecules to form single-molecule devices, which enable the detection of conductance data and monitoring of the interaction of bio-matter [35, 42, 43], such as the kinetics of DNA and protein activities. SWCNT is an outstanding material in molecular electronics. However, the inherent variability of SWCNTs [34, 38] and the sensitivity to the gate voltage [37] blocks the way to wider applications.

2.2.2 Graphene

In comparison with SWCNTs, graphene shows a homogeneous quality, and this two-dimensional material has the ability to be fabricated in high throughput without the gate dependence as well, making graphene a star material of electrodes [34, 37, 38].

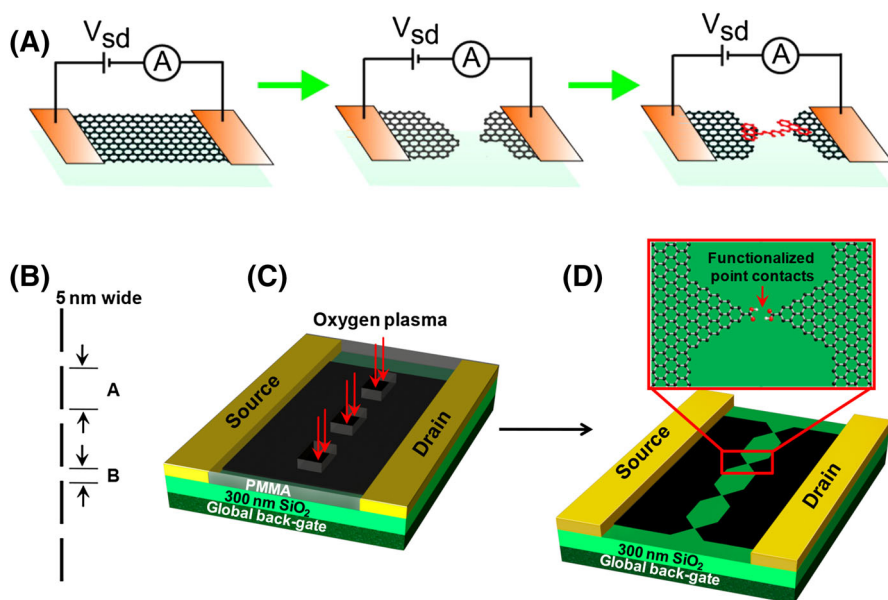


Fig. 4 **a** Depositing molecules inside a few-layer graphene nanogap, formed by feedback-controlled electro-burning. DLL method to form graphene point contacts arrays with gaps ≤ 10 nm. **b** A dashed line of 5-nm width; **c** using oxygen plasma to etch away graphene through the PMMA window; **d** point contacts arrays with gaps ≤ 10 nm with carboxylic acid-terminated. Reproduced with permission from Ref. [40]. Copyright 2011 American Chemical Society. Reproduced with permission from Ref. [34]. Copyright 2012 Wiley-VCH

In 2011, Prins [40] used a feedback-controlled electro-burning to form 1–2 nm gaps in graphene (Fig. 4a), then an anthracene terminated molecule was used to bridge graphene electrodes via π – π stacking. It showed a good gate controlled I – V characters in room temperature, exhibiting a simple gate-dependent switching effect of single-molecule devices based on graphene electrodes. However, the electro-burning process cannot be well controlled, and the number of molecules attached is not clear, making the devices unstable.

In order to overcome these problems, Cao et al. [34] developed a new method called “dash-line lithography” (DLL) to form graphene point contacts arrays with gaps of ≤ 10 nm. A DesignCAD file of a dash line (Fig. 4b) in a width of 5 nm was designed to open windows in PMMA. Then they used oxygen plasma to etch away the exposed graphene through the PMMA window (Fig. 4c). By applying gradual etching and undercutting of PMMA, graphene point contacts arrays were formed, with carboxylic acid on the ends (Fig. 4d). These carboxylic acid-terminated point contacts can covalently bond with molecules decorated with amines via amide linkages.

This covalent bond is robust enough to undergo chemical reactions, such as the coordination reaction. The molecules with a tridentate-aromatic pocket can coordinate with Co^{2+} ions (Fig. 5a). When the molecule-bonded devices were immersed in Co^{2+} solution, the devices behaved a high conductance state. Once

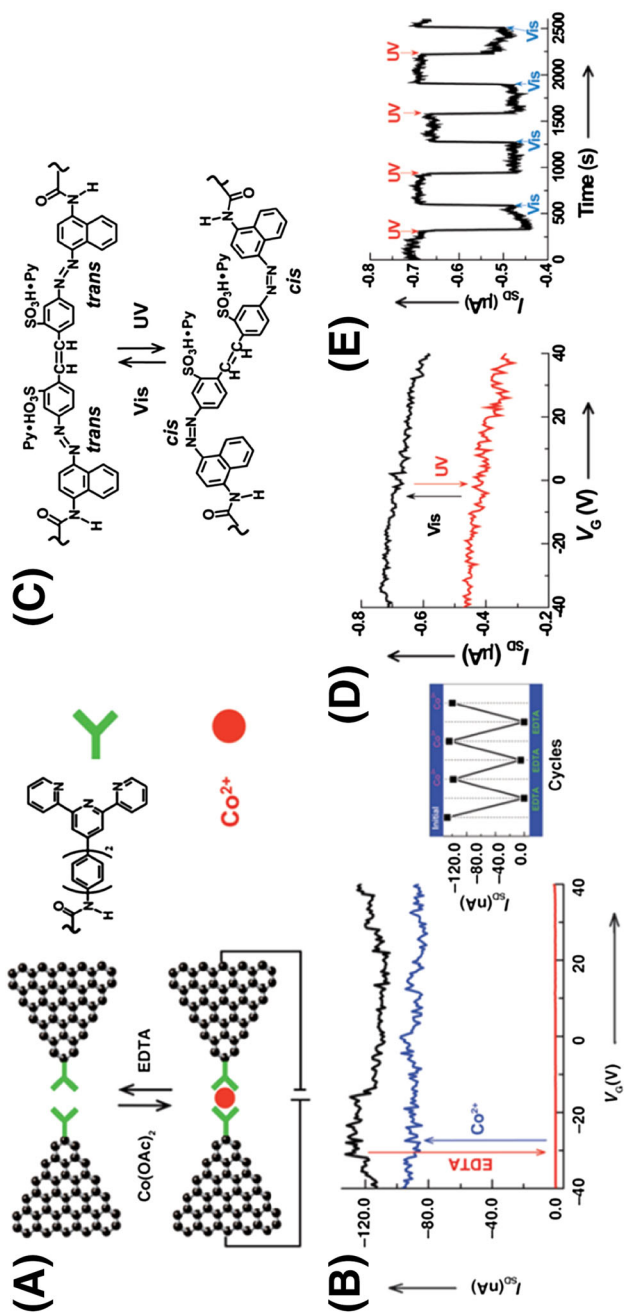


Fig. 5 **a** Schematic representation of the reversible coordination reaction. **b** Conductance cycles of the devices with alternate treatments of EDTA and Co^{2+} solutions. **c** Schematic representation of the azobenzene molecule in response to Vis and UV light. **d, e** Electrical characteristics of the graphene-azobenzene device. Reproduced with permission from Ref. [34]. Copyright 2012 Wiley-VCH. Reproduced with permission from Ref. [44]. Copyright 2013 Wiley-VCH

ethylene diamine tetra acetic acid (EDTA) was introduced to wash off the ions, the devices showed an off state with no current flow through. Figure 5b shows the conductance cycles of the devices, with a good stability, indicating the reproducibility and reliability of their devices. In their further investigation [44], by using the same DLL method, they built graphene-azobenzene devices, which can switch on and off in response to the irradiation of visible and UV light. Figure 5e shows the reversible photoswitching current. Compared with the pyrrole-based molecules covalently bonded with SWCNTs [45], these devices achieved a reversible photoswitching property. However, the devices cannot stay in an on state for a long time; once it was kept in darkness for 60 h, the current had a decrease. In addition to the photoswitching ability, these devices were sensitive to pH, owing to the two sulfonic acid groups. The conductance showed a switching cycle when alternatively immersed in the solution in low and high pH. These methods of creating functional molecular devices are useful for developing new devices with diverse functions and promoting the application of single-molecule devices.

In addition to different functional molecules, graphene-based electrodes can also be covalently connected with bio-matters. For the purpose of detecting metal ions, Gao et al. built graphene-enzyme devices [46]. The DNAzyme is sensitive to Cu^{2+} , which can split the substrate strand, producing an open circuit. These devices can detect Cu^{2+} ions even at the fM level. It may be further developed for real-time detection of various chemical and biological reactions. However, the device stability remains a challenge for biological connections. In future developments, the gap size and the electrode geometry will be the main challenges. Developing reliable methods with precise control of the electrode shape and gap size is a compelling obligation.

3 Single-Molecule Switches

The design and synthesis of switchable molecules are undoubtedly one of the great triumphs in the field of molecular electronics. Functional cores are usually modified with two anchoring groups for covalently binding to the electrodes and forming robust molecular junctions. Current methods for tuning electron transport are shown as follows: changing the electron transport pathway by triggering molecular conformation transitions (light-, mechanically, and chemically induced transitions) and tuning the molecular energy level. In detail, there are three ways of tuning the molecular energy level: (1) continuous excitation of molecular vibrations by electron carriers may induce switching (current-induced switching by inelastic scattering); (2) acting a sufficiently high electric field on a molecule may induce switching (field-induced switching); (3) heating of the molecular system may result in (non-selective) switching.

3.1 Conformation-Induced Switch

The conformational change between two or more stable states is a conspicuous switching pattern, which does not produce additional reactants or redundant products. Two principles should be considered: (1) conformational switches with molecules exhibiting different stable isomers, and (2) conformational switches with

molecular reorientation. The changes can be reversibly triggered by light, bias voltage, mechanical force, etc.

Light provides a noninvasive, easily addressable and cheap way for controlling the switches. Photochromic molecules, such as azobenzene [12], diarylethene (DAE) [5, 10], sipropyrin [47], dihydroazulene (DHA)/vinylheptafulvene (VHF) [11], and dimethyldihydropyrene (DHP)/cyclophanediene (CPD) [6, 9] derivatives, have been widely investigated in single-molecule devices and in solution. However, molecular properties in solvent and in the solid state are significantly different. The resonance effect between molecules and electrodes plays an important role. For example, in general, by exposing a DAE derivative to UV light, the devices represent a photoswitching behavior from the insulating state (off state) to the high conductance state (on state), which is due to the ring closure generating a conjugated pathway for electron transfer through the molecule. Dulic et al. built a one-way optoelectronic switch between gold electrodes using the MCBJ method [14]. They achieved DAE switching from the high-conductance state to the low-conductance (ring-opening process) state under visible light (546 nm). However, they failed to achieve the opposite process under UV illumination (313 nm). They explained that the presence of the gold quenched the excited state of the molecules in the open form. Different from gold electrodes, the lithography-defined oxidative cutting method was used to fabricate a single-molecule device with carbon electrodes [45]. This work used thiophene-based and pyrrole-based molecules as the functional cores (Fig. 6a). Thiophene-based molecules had a photocyclization as UV light was applied, resulting in an increase of current (Fig. 6b). The device could maintain a high-level conductance even without UV light, but it was unable to photochemically switch back. The pyrrole-based device had the ability to switch on under irradiation of UV light and thermally switch back in a dark condition overnight (Fig. 6c). Both molecules acted differently in comparison with their behaviors in solution. This may result from carbon electrodes, which might affect the energy structure of molecules when they are covalently bonded. This work gives a primary model of photoswitchable single-molecule devices, but the respond time and reversible switch remains obvious obstacles. Another work from Jia et al. [48] demonstrated the similar phenomenon. They covalently bonded DAE derivatives with graphene point contacts constructed by the DLL method. These DAE-graphene devices could switch from the off state to the on state. Taking both barrier and resonant tunneling models into consideration, the spectroscopic analyses proved the molecule–electrode coupling strength. This work also demonstrated a way that the investigation of new molecular structures can modulate the relationship between the charge transport mechanism and the electronic structure of molecular junctions. To reduce the strong conjunction between the photochromic core and the electrode, there are two feasible ways: (1) impairing the bonding strength by substituting the anchoring group with a weak bonding one; (2) modifying the linker group between the anchor and the functional core with unconjugated alkyl groups.

Broman et al. replaced sulfhydryl groups with MeS groups and realized reversible switching between DHA and VHF [11]. The bonding strength and the electron-transport mechanism can be experimentally tested. The stability diagram (Fig. 7) represents a set of characteristic Coulomb blockade diamonds, which

implies that the molecule is weakly coupled to electrodes and the transport through the molecule goes by sequential tunneling. However, weakly bonding leads to unsteady devices. An intrinsic contradiction of optimizing the device stability and molecular–electrode conjunction is inevitable.

In the most recent work, the strong conjunction problem has been solved by Guo's group [49]. By adding three non-conjugated CH_2 groups between the dithienylethene core and anchoring group NH_2 (Fig. 8a), a reversible light-induced single-molecule switch was achieved in graphene-based single-molecule junctions. They achieved building reliable switching devices with remarkable properties in the levels of accuracy (on/off ratio of ~ 100), stability (over a year), and reproducibility (46 devices with more than 100 cycles for photoswitching). This work demonstrated the importance of molecular engineering in modulating the molecule–electrode

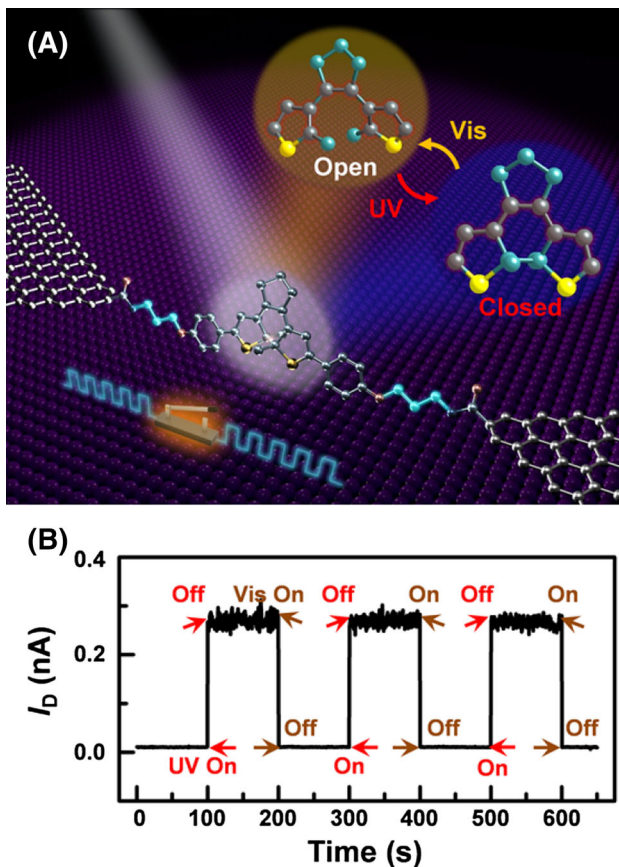


Fig. 8 **a** Schematic of a graphene based molecular junction that highlights the expansion of the molecular bridge by methylene groups. **b** Real-time measurements of the current through a diarylethene molecule that reversibly switches between the closed and open forms, upon exposure to ultraviolet (UV) and visible (Vis) radiation, respectively. $V_D = 100$ mV and $V_G = 0$ V. Reproduced with permission from Ref. [49]. Copyright 2016 AAAS

coupling strengths, and also proved that molecules with desired functionalities could be the key element for future molecular electronics.

Besides light illumination, mechanical force offers a novel tuning method that can trigger chemically inert molecules to present a switching behavior. This is due to the internal configuration change of the molecule or the interface conformation change between the electrode and the molecule. The mechanical force systems are usually fabricated by STM-BJ or MCBJ. The force can be controlled through the metal electrode distance in succession. Quek et al. [50] demonstrated reversible binary switching by mechanical control of the metal–molecule contact geometry in a 4,4'-bipyridine single-molecule junction. The conductance change was due to the distinct contact at the flexible but stable Au–N bond by first-principle calculation. The low conductance was derived from perpendicular between N-bond and conducting π -system. The on/off ratio of this device was approximately 10. In another attempt, oligosilanes showed reversible switching during mechanical tuning through stereoelectronic effect. The $(\text{SiMe}_2)_n$ ($n = 1-10$) oligosilanes, whose backbone have strong σ conjugation, are connected to the metal electrodes by methylthiomethyl linkers using STM-BJ [51]. Different from Quek's work [50], elongating the molecular junction led to a decrease of conductance and compressing the electrode led to an increase in conductance. As calculated by the DFT theory, the molecule had three terminal (C–S–C–Si) dihedral angles, which couple the electrode-linker orbital into the σ framework acting as a gate led to two conductive states (Fig. 9).

When a molecule has more than two anchoring groups, elongating the molecule not only causes the breaking of molecular junctions but also leads to the change of the anchoring points, which will change the electron transport pathway. Kiguchi et al. designed a covered quaterthiophene (QT) that has two thiophene ring anchors

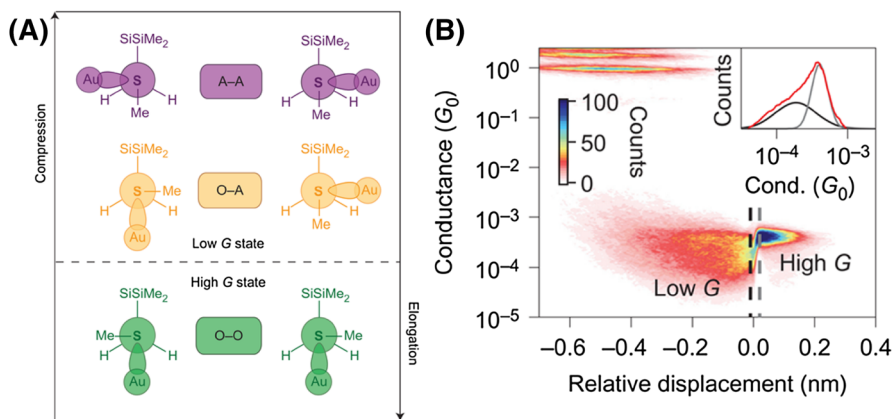


Fig. 9 a DFT calculations describing the mechanism for switching as the oligosilanes are elongated in the junction. A Newman projections for the A–A (purple), O–A (yellow), and O–O (green) dihedral configurations from the perspective of the sulfur–methylene σ bond in the Au–Si4–Au system. Junction elongation strains the molecule into the higher conducting O–O conformer. b Statistics of conductance curve measured in the Au–Si4–Au system, which demonstrates the conductance switching. Reproduced with permission from Ref. [51]. Copyright 2015 Nature Publishing Group

on each side and connected to the molecule using STM-BJ (Fig. 10) [52]. The single-molecule junction showed three distinct conductance states with values of $0.05 G_0$ (high), $0.005 G_0$ (medium), and $0.0005 G_0$ (low). Each conductance state corresponds to a pair of anchoring groups with distinct molecular lengths.

Chemical stimuli such as acid and base, metal ions, and chemical reactants can change the molecular conductance by tuning the conformation or setting off chemical reactions. Li et al. built a proton-triggered switch based on a molecular transistor with a novel edge-on gate [54]. The pyridinoparacyclophane (PPC) moiety was linked in the circuit using the STM-BJ method. The “on” and “off” switch could be reversibly set off by deprotonation and protonation of the pyridine ring. Further experiments focused on investigating the conductance of PCC with different substitutions of pyridine. The *para*-position of pyridine was functionalized with $-\text{NO}_2$, $-\text{Cl}$, $-\text{H}$, $-\text{OCH}_3$, and $-\text{N}(\text{CH}_3)_2$ (Fig. 11a). The conductance value of these protonated molecules remained consistent, which indicates the independence of the substituents on the pyridine ring. The switch mechanism was ascribed to the change in charge tunneling channels from HOMO in neutral molecules to LUMO in protonated ones.

Chemical reactants have an important effect on the device conductance, which in turn can show the reaction behavior of chemical reactants, offering a new way to understanding the mechanism of these chemical and biological activities. Different from the former studies, which bonded molecules in nanogaps between SWCNTs, Sorgenfrei et al. used an electrochemical oxidation to form point defects in carbon nanotube, then the probe DNA was covalently bonded there via an amide linkage [55]. This device could offer more rapid conductance change and higher yield because of the real-time monitoring while the point defects grew. By using an AFM tip to apply the gate voltage and combining the electrical data with spatial map, a scanning gate microscopy (SGM) was obtained to observe the defects. When the

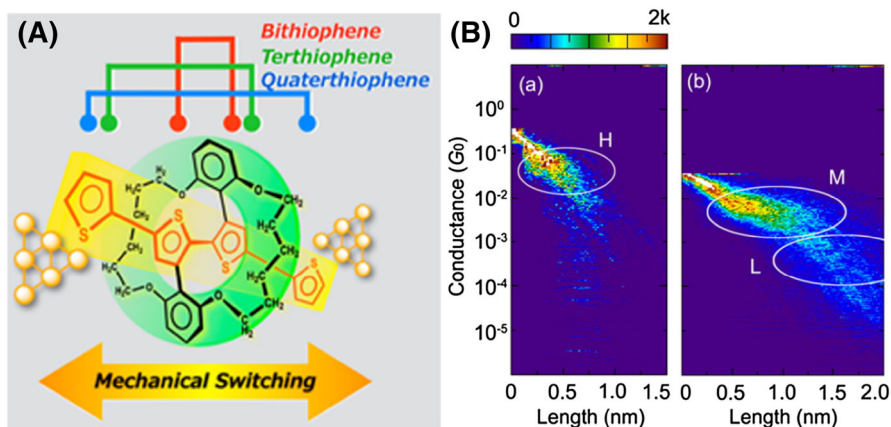


Fig. 10 **a** Schematic of mechanically induced quaterthiophene molecular junctions. **b** 2D conductance histograms constructed for *H*, and *M* and *L* conductance regimes, respectively; white circles are eye-guides to highlight *H*-, *M*-, and *L*-conductance states. Reproduced with permission from Ref. [53]. Copyright 2014 American Chemical Society

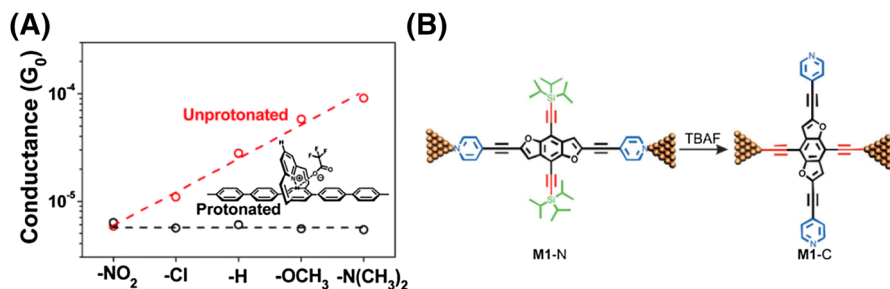


Fig. 11 a Conductance of protonated and unprotonated molecular junctions with different side groups. b Setting a course for molecular conductance along different pathways based on M1-N and M1-C. Reproduced with permission from Ref. [54]. Copyright 2016 The Royal Society of Chemistry. Reproduced with permission from Ref. [22]. Copyright 2015 Wiley-VCH

probe DNA was connected with target DNA, there was a conductance decrease (Fig. 12b), representing the off state of the device. On the contrary, when there was no target DNA, the device showed a high conductance, representing the on state (Fig. 12a). After the DNA combination, there were more detailed changes in the current, because of the conformational change of DNA. This study developed a single-molecule device with high sensitivity and high time resolution, showing the potential in kinetics monitoring of DNA and protein activities.

In 2012, Choi et al. attached a single lysozyme with SWCNT on the side wall via π - π stacking (Fig. 12c). Lysozyme is big enough to be identified by AFM (Fig. 12d), guaranteeing the single-molecule level [56]. Treating the device with peptidoglycan substrate made an increase of current (Fig. 12e), and the device showed a two-level random telegraph signal as a symbol of the single-molecule event. This device is stable with a temporal resolution into the single-microsecond regime, providing the basis of electrical monitoring of molecular dynamics.

Using the EBL to make SWCNT point contacts, Liu et al. [57] covalently bonded SWCNT electrodes with DNA, which were decorated with amine at the both ends. The DNA contained hydroxypyridone nucleobases (H) in the opposite position of DNA, as a flat bidentate ligand to form a stable metal-mediated base pair. The conductance of DNA increased with the number of H. Since the introduction of metal ions, which reinforce the π - π stacking of base-pairs in DNA, the conductance was improved. Because of the coordination of Cu^{2+} ions in DNA, they used a heated EDTA buffer to wash off Cu^{2+} ions, forming a metal-free DNA. This treatment resulted in a decrease in current, corresponding to the off state. Subsequently, after immersed in Cu^{2+} solution, the device gave out an increase in conductance. Alternately treating the device with EDTA and Cu^{2+} led to an on/off current switching circle. Similar conductance switching phenomenon was also found for other metal ions. This work indicated the potential of single metallo-DNA devices, which can act as reversible sensors of metal ions.

Huang et al. achieved irreversible control of the electrical conductance through changing the molecular orientation by selective gold electrode anchoring [22]. They rationally designed and synthesized a cruciform conjugated molecule with a benzo

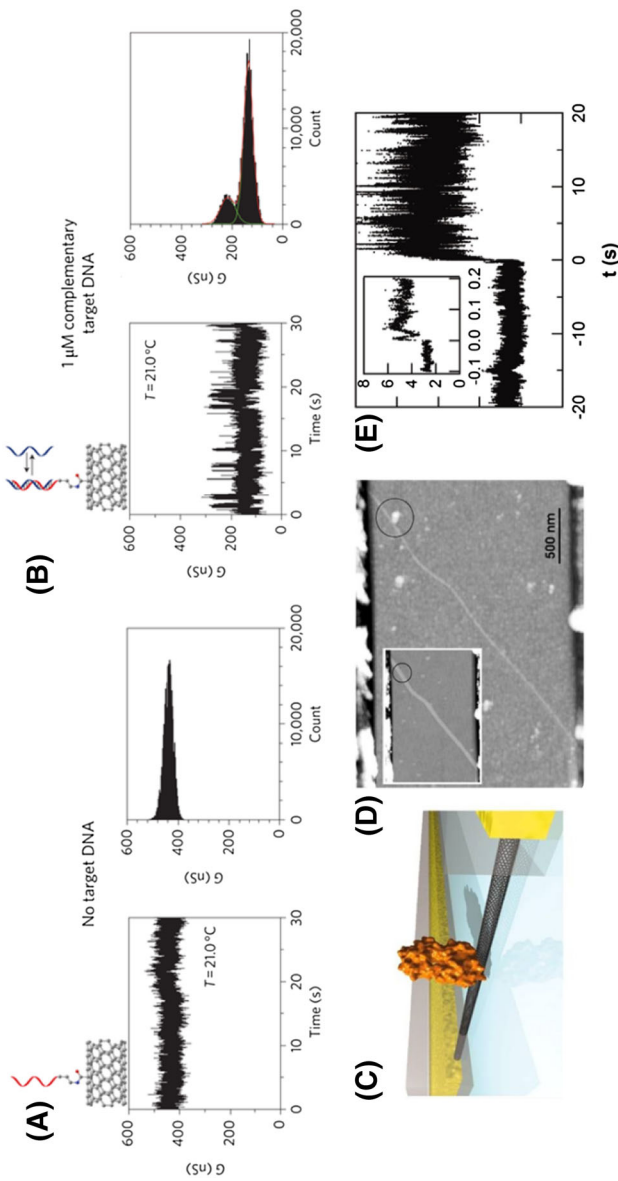


Fig. 12 **a, b** Conductance of the device without/with complementary DNA and the corresponding conductance-based histograms. **c** Schematic representation of lysozyme located on the SWCNTs. **d** AFM topography of a SWCNT device before and after treatment with lysozyme. **e** Addition of peptidoglycan substrate made an increase of current. Reproduced with permission from Ref. [55]. Copyright 2011 Nature Publishing Group. Reproduced with permission from Ref. [56]. Copyright 2012 AAAS

(1, 2-b: 4, 5-b') difuran core M1 (Fig. 11b). By adding tetrabutylammonium fluoride (TBAF), the protection group TIPS (TIPS = tri-isopropylsilyl) was cleaved in situ. A complete conversion from nitrogen atom-anchoring junctions to carbon atom-anchoring junctions was achieved and this led to more than an order of magnitude increase of the conductance. The conductance changing was attributed to the change between two electronic transport pathways.

3.2 Electrochemical Switch

Charging generally leads to notable changes in the molecular conductivity and can therefore be used as a switching mechanism. Molecular charging may occur via virtual occupation of an ionization level or by resonant tunneling to a molecular orbital, followed by geometric reorganization that stabilizes the charge state. Alternatively, it may result from external gating, which changes the energetic position of the molecular energy levels with respect to the Fermi level of the contacts, thus leading to charging.

There are two approaches for building a gate-controlled device. First, a third electrode can be added in a two terminal junctions. However, building a three-terminal electrode at the molecular level is a great challenge. In addition, an important limitation of solid-state three-terminal single-molecule devices is their low gate coupling ξ [58], being defined as the ratio between the molecular orbital energy shift ($E_{\text{HOMO/LUMO}}$) and the actual applied gate voltage (V_G). An alternative solution for this approach is to build a planar device, where an electrode gate is separated from the source-drain connects by a slight insulation film such as SiO_2 [24]. The second way is to import an electrochemical gate. In this approach, the

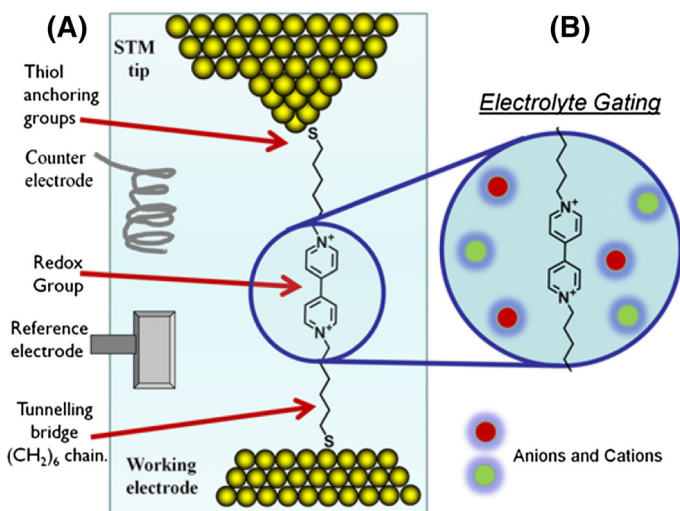


Fig. 13 Schematic diagram of the four-electrode cell (a) and the electrochemical double layer under a gate voltage (b). Reproduced with permission from Ref. [59]. Copyright 2015 American Chemical Society

molecular junction is immersed in an electrolyte, as shown in Fig. 13 [59]. The functional molecule was linked between the two metal electrodes, which can be viewed as the drain and source electrodes. The counter and reference electrode combination provided the gate electrode in this four-electrode bipotentiostat setup, with independent electrochemical potential control of the source and drain. Since the electrochemical electrode modulates the molecular bridge through the formation of an electronic double layer, it is presented as a more efficient alternative to control charge transport in a single-molecule electrical contact.

Molecules “wired” between single-molecule electrochemical junctions include redox active organic molecules, such as viologens [20], pyrrolo-tetrathiafulvalene (pTTF) [60], oligoanilines [61], oligothiophenes [62], unsubstituted and substituted oligo(phenylene ethynyls) (OPEs) [63, 64], ferrocene [65], anthraquinone [66, 67], perylene tetracarboxylic bisimide (PBI) [68, 69], benzodifuran [70], pyrrolidine-substituted perylenetetracarboxylic diimide (PTCDI) [71], redox-active proteins [72], and transition metal complex [73]. Some nonredox active molecules can also be adjusted by electrolyte gating, for example bispyridylethylene [74].

The intrinsic principle of electrochemical gating is to tune the energy level of the molecule. If the electrochemical potential is outside the HOMO–LUMO gap of the molecule, this apparently leads to charging of the molecule. If the molecule traps an electron (the LUMO level becomes available), this is a reduction process. Vice versa, if an electron is donated (or a hole is taken up, as the HOMO level becomes available), then the process is called oxidation [58]. An attempt for building an electrochemical control was achieved by Bahernejad et al. using an anthraquinone (AQ) center [52]. Two isomeric AQ-based derivatives, AQ-1,5 and AQ-1,4, were linked to molecular junctions by the STM-BJ technique (Fig. 14a–c). By varying the electrode potential over a range of ~ 1 V, the conductance had a changing with over an order of magnitude. At the redox potential, changing in redox state leads to reversible conductance switching. This was accompanied by changes in conjugation pattern from linear (reduced state) to cross-conjugated (oxidized state). These observations were supported by DFT-based transport calculations.

Gating effect is a crucial parameter for an electrochemical gating. Li et al. correlated the molecule/electrode contact resistance to the electrochemical gating effect [70]. They studied a benzodifuran core-based single-molecule redox switch in HClO_4 electrolyte using both STM-BJ and MCBJ methods. An anchoring group effect had also been tested (Fig. 14d–f). The on/off ratio rose from 2.5 to 8 when using CS_2^- group to replace thiol group. These results showed that we could improve the gating effect by reducing the resistance between electrodes and molecules.

By changing aqueous electrolyte into ionic liquid, Osorio et al. quantitatively investigated the gating difference between aqueous electrolyte and ionic liquid. They constructed a single-molecule electrochemical gating of a viologen molecular bridge in 1-butyl-3-methylimidazolium triflate (BMIM-OTf) [59]. A hard gating with gate-coupling efficiency $\xi = 1$ was found in ionic liquid, while a soft gate with $\xi < 0.2$ was found in aqueous solution. Since the gating coupling is controlled by electrostatic interactions between the double layer gate and the redox bridge, its efficiency might be expected to depend on both of these components and vary

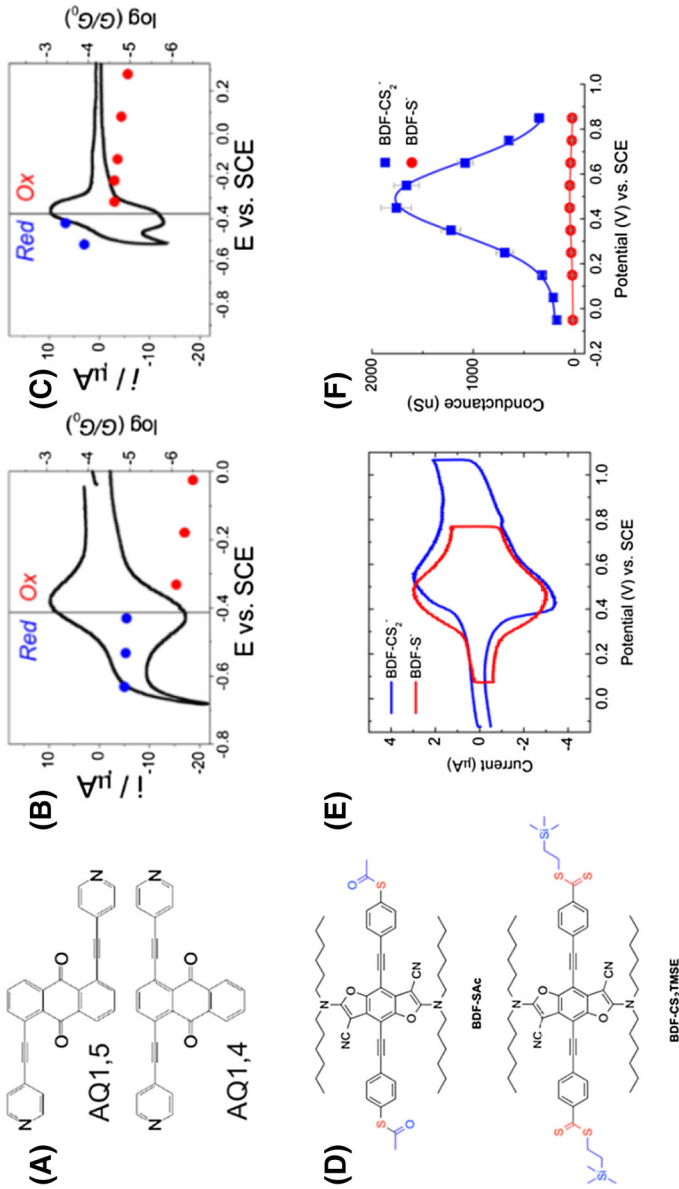


Fig. 14 **a** Molecular structure of AQ-1,5 and AQ-1,4. Experimental molecular conductance as a function of the applied gating potential vs. SCE for AQ-1,5 (**b**) and AQ-1,4 (**c**). **d** Molecular structure of two benzodifuran derivatives. **e** Cyclic voltammograms of BDF-S-(red) and BDF-CS₂-(blue) on Au(111) electrodes in 0.1 M HClO₄. Scan rate: 0.5 V s⁻¹. **f** Single-molecule conductance of BDF-S-(red circles) and BDF-CS₂-(blue squares) as a function of gating (substrate electrode) potential determined from STM-BJ experiments. Reproduced with permission from Ref. [52, 70]. Copyright 2014 American Chemical Society

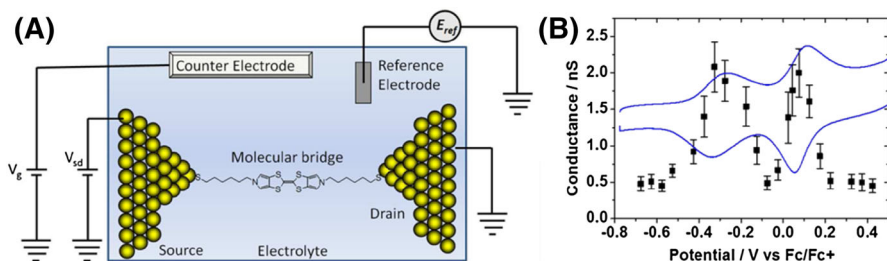


Fig. 15 **a** An electrochemical molecular break junction with electrolyte gating. **b** Plot of conductance of pTTF against the sample electrochemical potential (with $V_{\text{bias}} = +0.6$ V, black point) and a cyclic voltammogram (blue line) of a pTTF monolayer. Reproduced with permission from Ref. [59]. Copyright 2012 American Chemical Society

between redox systems. A similar trend can be seen in the data for a redox active pyrrolo-tetrathiafulvalene bridge, with a gate coupling of $\zeta = 0.8$ –1 in ionic liquid in comparison with a lower value ($\zeta = 0.5$) in aqueous solution. Kay et al. investigated redox-active pTTF moieties in room-temperature ionic liquid (RTIL) [60]. Compared with aqueous solution, RTIL is more stable, which enables the study of molecular conductance over a much wider electrochemical potential range. pTTF first switch to its monocationic state (pTTF⁺) and then to its dicationic state (pTTF²⁺) (Fig. 15).

The charge-transport mechanism can be described as a two-step Kuznstzov–Ulstrup Model (Fig. 16). In this model, charge is transported (“hops”) through either the reduced or oxidized state of the molecule. First, the redox center reorganizes through environmental and internal fluctuations in order to let the relevant molecular orbitals approach the Fermi level of one electrode. Charge is then transferred onto the redox center through a Franck–Condon-type transition. It is accompanied by partial vibrational relaxation and subsequent charge transfer to the other electrode in the adiabatic limit. In this partially relaxed state, many electrons or holes can transfer across, benefiting to the enhancement in the junction current seen close to the reversible potential. In contrast, in the weak-coupling (diabatic) limit, complete vibrational relaxation occurs before the electron/hole transfers to the second electrode, and current enhancement is minimal.

Besides electrolyte environment, a local microenvironment also has a large impact on the molecular conductance. In a recently work, Zhang et al. used Cucurbit(8) uril to host the viologen (bipyridinium), forming a 1:1 supramolecular complex [20]. The experimental result showed that the conductance of viologen derivatives increased upon encapsulation within the hydrophobic CB(8) cavity. This can be explained by reduced outer sphere reorganization energy within the framework of Marcus-type model for electron transfer.

The electrochemical gating method provides an effective method for tuning the energy level of a single molecule and further results in the redox reaction and corresponding switching effect. Great efforts have been made in tuning different kinds of functional molecules and optimizing the device performance. Miniaturization of this four-electrode system and finding applications will be the next step in this field.

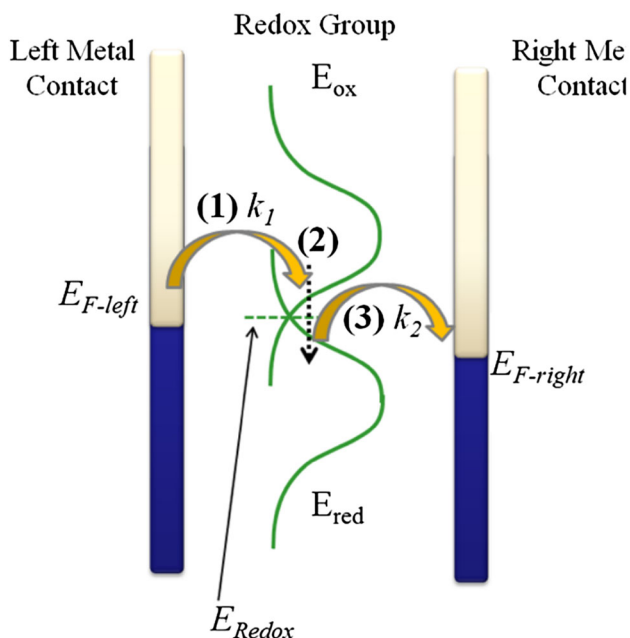


Fig. 16 KU model. The first step of charge transfer occurs when the HOMO is close to the Fermi level of the “left-hand” gold electrode, and involves hole tunneling to the HOMO of the molecular bridge (or electron tunneling from the HOMO). The oxidized and vibrational group relaxes toward the Fermi level of the “right-hand” gold electrode. Reproduced with permission from Ref. [59]. Copyright 2012 American Chemical Society

3.3 Electron Spin Tuning-Based Switch

Spintronics utilizes the spin degree of freedom of electrons to transfer and manipulate information, thus offering low-power and high-speed electronic devices. Electron spin tuning can be operated in two ways: one is to contact organic molecules between two ferromagnetic electrodes, called the spintronic progress, and the other is to use a molecule with a tunable spin state that can be triggered by the spin crossover effect. Transporting spin electrons through organic molecules takes advantage of the weak spin–orbit and hyperfine interactions in the organic compound. This leads to the possibility of preserving spin coherence over time and distance much longer than in conventional metals. For unpaired spins, the Kondo effect has been observed at a low temperature anomaly at small voltage.

In a previous work, the idea of using organic molecules as spin valves with large magnetoresistance ratios has been proven theoretically to be feasible by using non-equilibrium transport methods and density functional theory [75]. Either *n*-octanedithiolate or 1,4-*n*-phenyl-dithiolate was analyzed with a nickel connect. The octane molecule had a tunneling-like transport behavior and an order of magnetoresistance. For the case of transport through molecular states extending throughout the entire molecule (1,4-*n*-phenyl-dithiolate), much larger magnetoresistance can be achieved.

This can be attributed to the strong current suppression in the antiparallel configuration due to the spin-selective coupling of the molecule with the leads.

A novel single-radical molecular junction, which has a large magnetoresistance, was successfully done by Hayakawa et al. [76]. An oligo(*p*-phenyleneethynylene) (OPE) backbone, {4-((2,5-bis(4-sulfanylphenyl(eth-1-yn-2-yl))phenyl)carbonyl) (methyl)amino)-2,2,6,6-tetramethylpiperidin-1-yl}oxidanyl (TEMPO-OPE), was placed on an Au electrode by using the MCBJ method at 4.2 K (Fig. 17). Substantially, MRs of 16–278% were observed at 4 T while MRs in non-radical OPE were only found to be 2–4%. The unpaired electron can reduce the coupling of the current-carrying molecular orbital with metal electrodes, which results in large MRs for TEMPO-OPE.

Spin crossover (SCO) phenomenon can lead to the bistability, which has been observed in some metal-containing molecules. The most investigated metal ion Fe(II) can be used as an example to illuminate the principle of electron configuration. When the iron atom is surrounded by an octahedral ligand environment, its five spin-degenerate 3d levels will be split into a doublet and a triplet. The filling order of these levels with the six electrons of Fe(II) depends on the ratio between the ligand field energy, E_{LF} , and the spin exchange energy, E_{EXC} . If $E_{LF} \gg E_{EXC}$, electrons are all paired up and the triplet is completely filled. This case is defined as the low-spin (LS) state, which gives a total spin $S = 0$. Inversely, if $E_{EXC} \gg E_{LF}$, the levels are filled based on Hund's rule and the spin reaches a maximum value, $S = 2$. This case is defined as the high-spin (HS) state. The E_{EXC}/E_{LF} ratio can be adjusted by external stimuli such as pressure, temperature, and mechanical force. In addition to the total spin, the LS and HS states present the difference in geometry, electronic structure, and HOMO–LUMO gap energy. According to the theoretical prediction, in general the HS state has a higher conductance than the LS state.

Frisenda et al. have studied a mechanically Fe(II) spin crossover switches by using a MCBJ technique [77]. Two terpyridines form an orthometric coordination under the relaxation condition and the electron was in a low-spin state (Fig. 18).

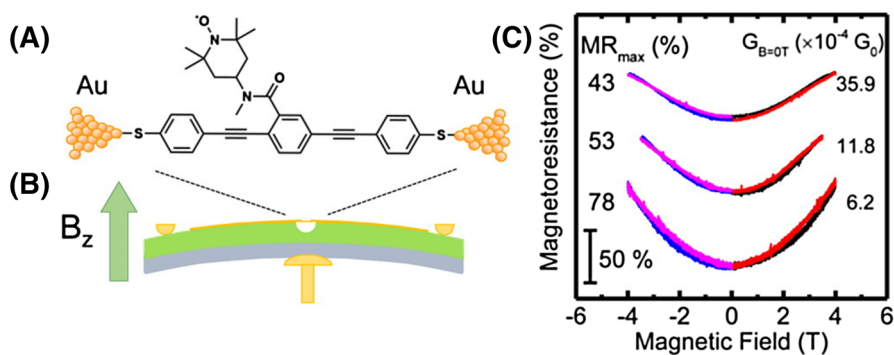


Fig. 17 Schematic illustration of single-molecule junctions for TEMPO-OPE (a) and pristine OPE (b). c Magnetoresistance curves from TEMPO-OPE molecular junctions. Reproduced with permission from Ref. [76]. Copyright 2016 American Chemical Society

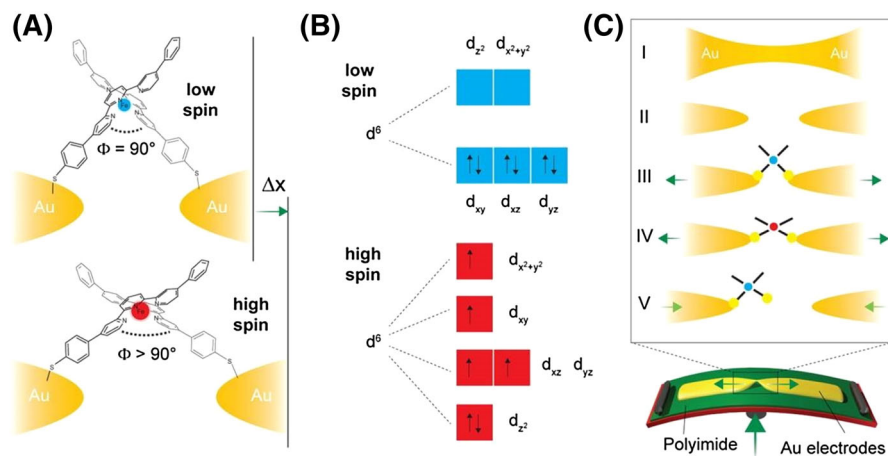


Fig. 18 **a** Sketch of a Fe(II)-based SCO molecular junction in the ideal arrangement to trigger the LS to HS switch by separating the electrodes by Δx . **b** Fe(II) 3d levels involved in the spin-crossover phenomenon. **c** Schematic illustration of a MCBJ setup (*bottom*) with the molecule placed in the junction as sketched in **a**. Reproduced with permission from Ref. [77]. Copyright 2016 American Chemical Society

When elongating the gap between two electrodes, the molecule got stretched, reaching a coordination angle larger than 90. The current had a two-orders-of-magnitude increase in this process. This can be explained by switching the LS state to the HS state.

Apart from setting up a transition metal ion in the electron transport pathway, which can directly tune the current, a magnetic coupling path can also be orthogonally oriented to the conductance channel. Wagner et al. synthesized a molecule modulated by two cobalt ion centers [78]. They found a bias-driven switching, which has been assigned to the transition from the pseudo-singlet of the ground state of a coupled spin system to a pseudo-triplet state at a higher bias voltage. Aragonès et al. built a junction by bridging individual Fe(II) SCO complexes, $[\text{Fe}(\text{tzpy})_2(\text{NCS})_2]$, with high- and low-spin states between a gold electrode and a magnetically polarized nickel electrode [79]. The switching mechanism was based on spin-dependent transport in a single-molecule device that results in the strong interaction of a paramagnetic molecule with heavy-metal surface atoms. This switch led to a large conductance switch (>100) at room temperature.

Another nickel electrode-based single-molecule device was investigated by Brooke et al. [80]. They integrated a non-redox active molecule 4,4'-bipyridine (44BP) into two Ni electrodes by using STM-BJ and electrochemical gating. The conductance and gain of the resulting Ni–44BP–Ni electrochemical transistor was significantly higher than an analogous Au-based device. Ab initio calculations revealed that this behavior arose because charge transport was mediated by spin-polarized Ni d-electrons, which hybridize strongly with molecular orbitals to form a “spinterface”.

3.4 Other Switching Mechanisms

Except for the classic mechanisms, switching phenomena such as stochastic switching and charge-state alteration have also been found in the recent work. A field (bias voltage)-induced conductance switching was found by Schwarz et al. [19]. Three organometallic compounds, which had individual metal centers (Fe, Ru, Mo) in the transport pathway, were studied. The I - V curves of single-molecule devices fabricated by MCBJ could be classified by two types. The first type was found for all compounds and was characterized by a small hysteresis that affected only a particular section of the voltage. The conductance gap was not altered, and the transition between the curves was continuous. The second type of curves was only observed for Mo compounds and distinct from the first type by a lower current and an abrupt switching (on/off ratio ~ 1000) between two distinct curves, accompanied by an obvious hysteresis. The conductance gaps changed substantially (from 0.15 to 0.85 V). Theoretical results showed that bias-driven charging indicated an oxidation/reduction mechanism mediated by a weakly coupled, localized molecular orbital that is unique to the Mo compound because of its spin-polarized ground state. Raising bias voltage can also apply a force on the dipole of an asymmetric molecule that can reorient the molecule from the ground state (“off”) into a metastable configuration (“on”) and back [81].

In some cases, stochastic switching was observed. This phenomenon was firstly investigated in self-assembled monolayer (SAM) systems. Through a room-temperature STM system, the oligo(phenylene ethynylene) (OPE) was found to show stochastic switching and remain the effect when the side group of OPE was changed [82]. Further experiments showed that molecules with higher degrees of conformational freedom exhibited higher switching rates. A supposed explanation for these results was given when the authors observed stochastic switching in simple alkanedithiols embedded in alkanethiolate SAMs. The authors argued that the switching was caused by changes in the Au-S bond between the molecules and the gold substrate rather than internal molecular electronic changes. In single-molecule junction systems, a temperature-dependent stochastic switching effect has been demonstrated in a graphene-diarylethene-graphene junction (Fig. 19) [49]. This phenomenon was observed only for the closed form in the temperature range of 160–240 K. The stochastic switching was attributed to DAE conformational change, possibly driven by molecular charging, which means changing occupation of the molecular HOMO. Consequently, two mechanisms have been proposed to explain stochastic switching: (1) molecular motion due to the conformational changes; (2) bond-fluctuation due to the attachment/detachment process of the molecules tethered to the gold surface in a random manner [83].

3.5 Multiple Responses

We have discussed different kinds of molecular switches above. One goal in the field is to build a “molecular chip” by using integrated molecular switches. There are two strategies for integrating these switches into the electrical circuit. The first way is to install several molecular switches in series in the same molecular junction.

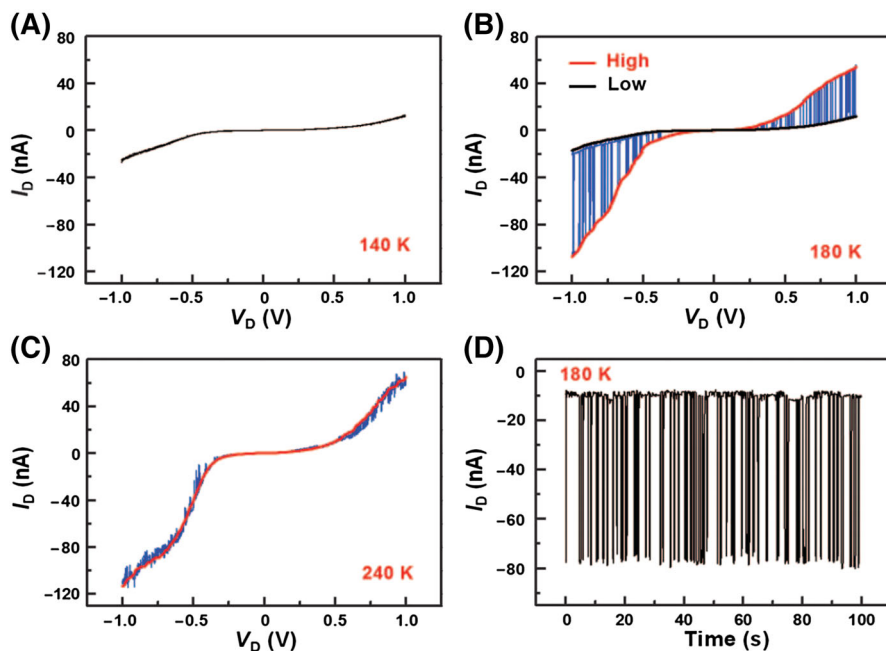


Fig. 19 Temperature-dependent stochastic switching of graphene–diarylethene–graphene junctions. **a** I – V characteristics of a single diarylethene junction in the closed form screened at 140 K for at least three times, which did not show stochastic switching. **b** Stochastic switching between two conductive states at 180 K. **c** I – V characteristics at 240 K. The stochastic conductance switching started to disappear at this temperature. **d** Real-time recording of stochastic conductance switching at 180 K, with a source-drain bias of -0.8 V and a gate voltage of 0 V. Reproduced with permission from Ref. [49]. Copyright 2016 AAAS

Another way is to integrate molecular junctions. However, the latter method needs extensive accurate control at the molecular level. The former method was studied by Meng et al. [84, 85]. The orthogonally modulated molecular transport junctions were achieved via chemically fabricated nanogaps (on-wire lithography) functionalized with DAE units bearing organometallic ruthenium fragments (Fig. 20). The stepwise control of molecular isomerization can be repeatedly and reversibly completed with use of orthogonal electrochemical and optical stimuli to realize the controllable switching of conductivity between two distinct states. An electronic logic gate can be achieved such as two-input OR and a three-input AND–OR, proving that rational chemical design can lead to multifunctional molecular devices. There are limitations in this molecular device: the molecular gap fabricated by on-wire lithography is an ensemble molecular gap which can only show ensemble average molecular characteristics. What's more, response time of the devices is in a range of 30 min resulting from ensemble properties of the devices. Another multi-responsive single-molecule switch triggered by photon and chemical stimuli was fabricated by Darwish et al. [47]. They designed the switch by using a spiropyran center, which is responsive to many kinds of stimuli such as light, solvent, metal ion, gas, acid, and base.

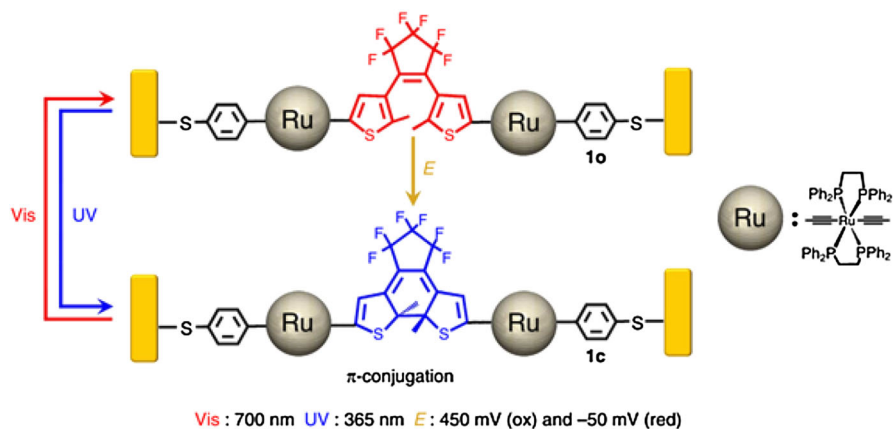


Fig. 20 Schematic of molecular isomerization under external control. Reproduced with permission from Ref. [84]. Copyright 2014 Nature Publishing Group

4 Film-Based Switches

The film formed by organic molecules can be used as a smart surface [86], which is able to respond to external stimuli. According to the types of stimulus, different molecules were designed to achieve multiple functional devices. Organic molecules with their own features, such as photochemically and electrochemically switching abilities, can be combined together, affording molecules with various functions and thus forming multifunctional films.

For example, DAE is a photo and electrochromic unit with the multi-functions. It was the most commonly used key element for building smart surfaces. In 2012 [87], the DAE unit was combined with polymerizable groups, in the presence of phenyl spacers, which ensured their functionality that electronic-redox switching can be achieved in polymer electrodes. The electro-polymerization process can be realized and remain stable in open air, having a potential in future applications of closed electronic devices. DAE films can also be applied in photoswitchable devices [88, 89]. They can absorb UV light to form a closed state and visible light to an open state. The conductance of this device showed repeated conductance switching when UV and Vis lights were alternatively introduced to illuminate the DAE film.

This phenomenon was well investigated by using STM when DAEs were inserted into a monolayer of dodecanethiol (Fig. 21a) [90]. DAE has two states (Fig. 21a), which shows a bright spot with a higher configuration. When UV and Vis light were interacted in turn, the reversible switching behavior of individual molecules was observed in STM images (Fig. 21c). The variation of height was also consistent with the experiments. This work gave us a clear image of the reversible change of DAE, offering a better understanding of DAE ensemble phenomena.

When the DAE unit was combined with a chiral unit [90], the molecular layer can show reversible colors with the irradiation of UV and Vis light, exhibiting a new way in developing functional devices. Amphiphilic photochromic DAE [91] can also be achieved by decorating the photochromic DAE unit with a cholesterol unit

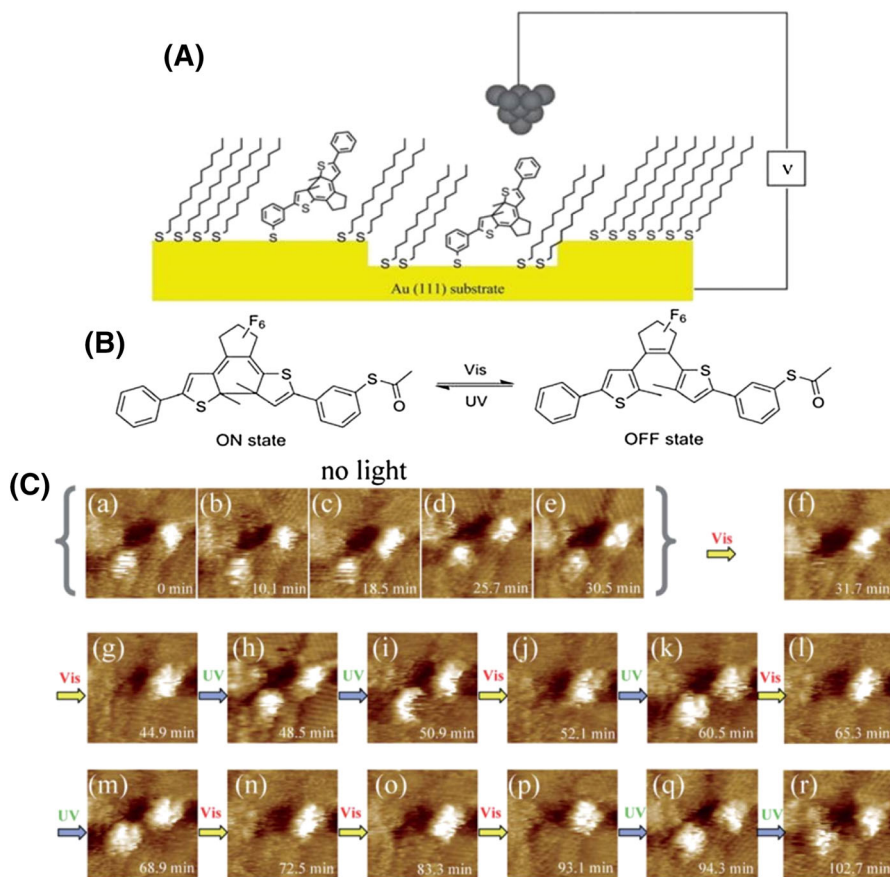


Fig. 21 **a** Individual DAE molecules were located within a self-assembled monolayer of dodecanethiol. **b** Schematic diagram of the on and off states of DAE. **c** Reversible switching behaviors of individual molecules. Reproduced with permission from Ref. [90]. Copyright 2013 Royal Society of Chemistry

(providing hydrophobic functionality) and a poly (ethylene glycol)-modified pyridinium group (providing hydrophilic functionality). This molecule reacted to UV and Vis light with configuration changes (Fig. 22a), which result in a transformation of hydrophobicity/hydrophilicity, showing different dynamic self-assembly behaviors in aqueous (Fig. 22b) and organic media (Fig. 22c). This allowed photocontrolled vesicle formation in water and self-assembly of organ-gel fibers in organic media. This research exhibited the potential use of DAE in photocontrolled chemical release systems.

The various functionalities and fundamental understanding of DAEs offer a remarkable symbol of functional molecules, fostering the rapid development of this field towards practical application. Functional molecules with a revisable switching effect can be applied between metal electrodes, which have a screening of the field effect, resulting in inefficient switching and poor on/off ratio [92]. On the contrary, the low-dimensional carbon material only screens the gate field in junction regions.

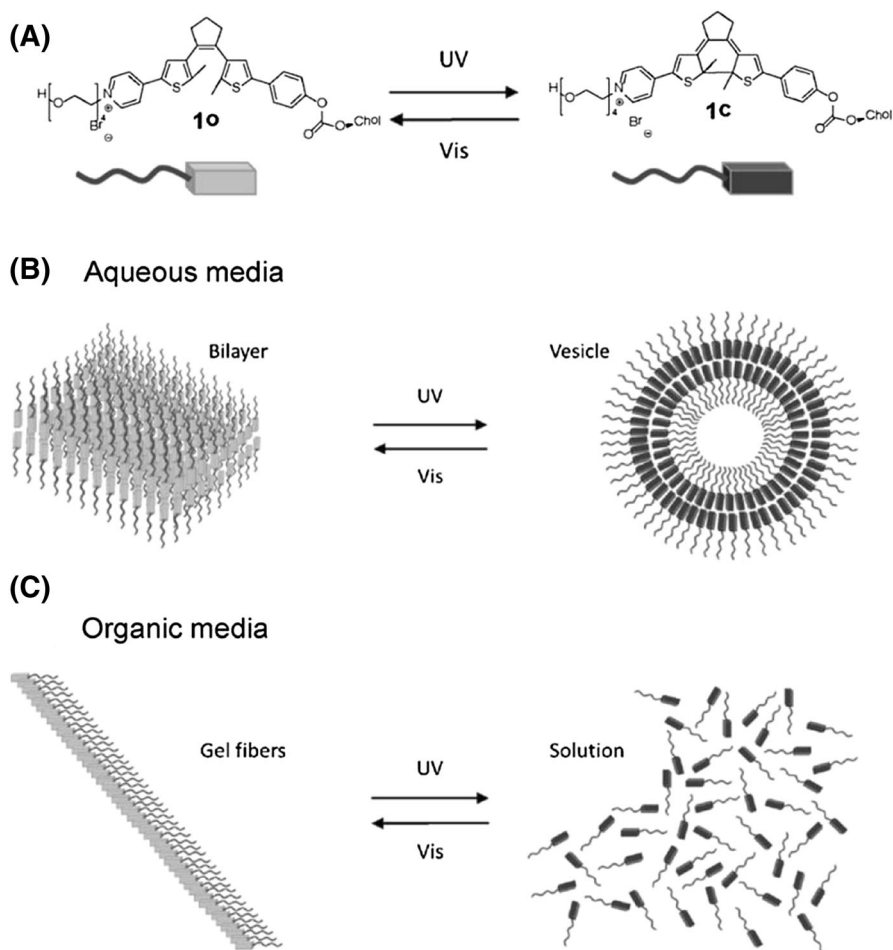


Fig. 22 a Open and closed forms of decorated DAE. b, c Light-induced dynamic self-assembly behaviors of decorated DAE. Reproduced with permission from Ref. [91]. Copyright 2014 Wiley-VCH

Hence, the gate regulation can be more efficient with high on/off ratio. For example, hexabenzocoronenes (HBCs) were chosen as a monomer to form monolayers in a self-assembled way between SWCNT electrodes with a current on/off ratio of $\sim 10^5$. HBC can also react to environment stimulus such as temperature and photon. The combination of top-down fabrication and bottom-up self-assembly gave a new way in constructing molecular devices, showing a new device type of environmental and chemical sensing.

By using the similar method, a water-processed copper phthalocyanine (CuPc) monolayer was used with SWCNT electrodes for high sensitive photo-detector [93] at room temperature, with responsivity greater than 10^8 A W^{-1} , detectivities greater than 7×10^{15} Jones.

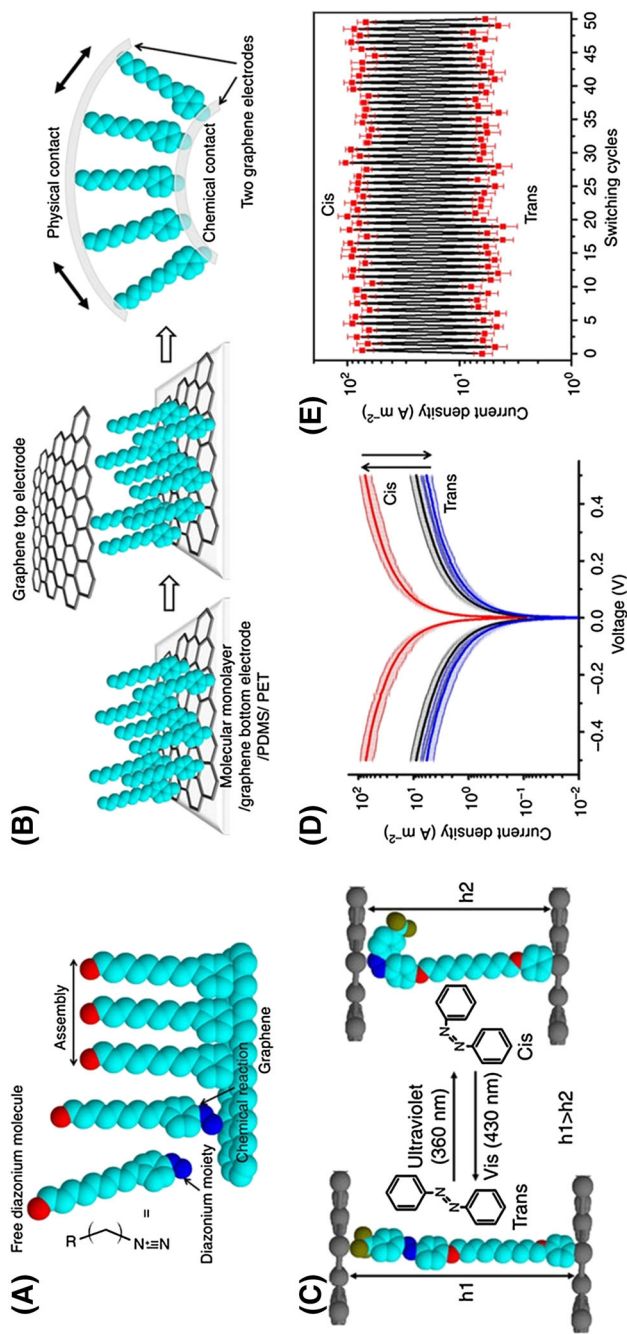


Fig. 23 **a** Self-assembled process of aryl diazonium molecules on graphene. **b** Schematic diagram of transparent and flexible devices based on graphene electrodes. **c** Molecular transmission distance ($h1$, $h2$) corresponding to molecular conformation in reaction to light irradiation. **d** Current characteristics of a device. **e** Changes in current density of the device. Reproduced with permission from Ref. [97]. Copyright 2013 Nature Publishing Group

In comparison with SWCNTs, graphene electrodes exhibit outstanding interface contact with organic molecules, and its humongous electric character offers higher stability and will not be influenced by gate regulation, making it suitable for molecular electronics. Cao et al. used graphene sheets as electrodes to measure the electrical conductance of poly (3-hexylthiophene-2,5-diyl) (P3HT) [94]. This device had responsivity as high as 8.3 A W^{-1} and on/off ration of 10^5 . This device also showed reversible photocurrents by switching on/off light, offering a new application in developing integrated ultrasensitive devices. In 2010, CuPc LB monolayers were applied with single-layer graphene electrodes [95], with a carrier mobility of $0.04 \text{ cm}^2 \text{ v}^{-1} \text{ s}^{-1}$, an on/off ration current ratio over 10^6 , and the best responsivity of about $7.1 \times 10^5 \text{ A W}^{-1}$. This similar fabrication method [92] with graphene electrodes gives new material options in future devices.

With the development of molecular devices, the wearable device is drawing increasing attention [96]. Graphene as an intrinsically transparent, conductive, and flexible electrode meets the need of wearable devices. In 2013, Seo et al. reported a photo-switchable device with highly transparency and flexibility [97]. They used aryl diazonium compounds, which undergo a self-assembled process on graphene electrodes, and the diazonium unit was covalently connected with carbon atoms in the graphene plane (Fig. 23a). On the other side, a layer of graphene as top electrode was connected with molecular monolayers by physical contact (Fig. 23b). This vertical device combined chemical and physical contact together and maintained the good conductance as well as high flexibility. Since the molecule has UV/Vis absorption, its configuration can switch with light induction (Fig. 23c). Figure 23e shows the reversible current of this device with good stability. Unlike the traditional electrodes [94, 95, 98], this vertical structure provides a new way in flexibility devices.

5 Conclusion

The switching effect is an essential phenomenon in our daily life. Design and fabrication of switchable devices with good stability and reproducibility is of great importance to the development of the field of nano/molecular electronics. In this review, metal- and carbon-based molecular junctions were discussed. Carbon electrodes have unique characteristics, promising the potential of carbon era after silicon. On the other hand, as the essence of functionality in the material world, molecules exhibit numerous characteristics. Understanding and using these unique qualities is the goal we are pursuing. To this end, conformation transformation, electrochemical gating, and electron spin tuning are mostly used as the intrinsic mechanism for explaining the intrinsic molecular switching effect. Different triggers, such as light, mechanical force, bias voltage, gating, and chemical reactant, have been proven suitable for particular situations. Molecular film-based devices provide us the nature of the ensemble, while single-molecule devices offer a way to learn the rich information hidden in the ensemble at the single-event level. The combination of reliable electrodes with functional molecules creates new opportunities to achieve remarkable electrical characteristics. However, there are still

some challenges that need to be overcome. The stability and reproducibility of molecular devices remain challenging. An electrode with controllable configuration is the foundation of molecular devices. Hence, new methods for precise formation of molecular junctions are crucial. The contact interface between molecules and electrodes is also of great importance to modulate the transport characteristics of molecular devices. Therefore, further investigation of the contact interface should be done to solve this problem. In addition to these, as the detailed mechanism of molecular conformational changes or biomolecular interactions is not fully understood, the development of more stable and reliable molecular devices is in great need.

Acknowledgements This work was supported by the National Natural Science Funds of China (21225311, 91333102, and 21373014) and the 973 Project (2012CB921404 and 2012CB921403).

References

1. Xiang D, Wang X, Jia C, Lee T, Guo X (2016) *Chem Rev* 116:4318
2. van der Molen SJ, Liljeroth P (2010) *J Phys Condens Matter* 22:133001
3. Zhang X, Hou L, Samori P (2016) *Nat Commun* 7:11118
4. Taherinia D, Frisbie CD (2016) *J Phys Chem C* 120:6442
5. Sendler T, Luka-Guth K, Wieser M, Lokamani, Wolf J, Helm M, Gemming S, Kerbusch J, Scheer E, Huhn T, Erbe A (2015) *Adv Sci* 2:1500017
6. Hu W, Zhang G-P, Duan S, Fu Q, Luo Y (2015) *J Phys Chem C* 119:11468
7. Tsuji Y, Hoffmann R (2014) *Angew Chem Int Ed* 53:4093
8. Zheng YB, Pathem BK, Hohman JN, Thomas JC, Kim M, Weiss PS (2013) *Adv Mater* 25:302
9. Roldan D, Kaliginedi V, Cobo S, Kolivoska V, Bucher C, Hong W, Royal G, Wandlowski T (2013) *J Am Chem Soc* 135:5974
10. Kim Y, Hellmuth TJ, Sysoiev D, Pauly F, Pietsch T, Wolf J, Erbe A, Huhn T, Groth U, Steiner UE, Scheer E (2012) *Nano Lett* 12:3736
11. Broman SL, Lara-Avila S, Thisted CL, Bond AD, Kubatkin S, Danilov A, Nielsen MB (2012) *Adv Funct Mater* 22:4249
12. Martin S, Haiss W, Higgins SJ, Nichols RJ (2010) *Nano Lett* 10:2019
13. Choi BY, Kahng SJ, Kim S, Kim H, Kim HW, Song YJ, Ihm J, Kuk Y (2006) *Phys Rev Lett* 96:156106
14. Dulic D, van der Molen SJ, Kudernac T, Jonkman HT, de Jong JJ, Bowden TN, van Esch J, Feringa BL, van Wees BJ (2003) *Phys Rev Lett* 91:207402
15. Lin W, Zhao Q, Sun H, Zhang KY, Yang H, Yu Q, Zhou X, Guo S, Liu S, Huang W (2015) *Adv Opt Mater* 3:368
16. Sun H, Liu S, Lin W, Zhang KY, Lv W, Huang X, Huo F, Yang H, Jenkins G, Zhao Q, Huang W (2014) *Nat Commun* 5:3601
17. Zhang KY, Chen X, Sun G, Zhang T, Liu S, Zhao Q, Huang W (2016) *Adv Mater* 28:7137
18. Rascón-Ramos H, Artés JM, Li Y, Hihath J (2015) *Nat Mater* 14:517
19. Schwarz F, Kastlunger G, Lissel F, Egler-Lucas C, Semenov SN, Venkatesan K, Berke H, Stadler R, Lortscher E (2016) *Nat Nano* 11:170
20. Zhang W, Gan S, Vezzoli A, Davidson RJ, Milan DC, Luzyanin KV, Higgins SJ, Nichols RJ, Beeby A, Low PJ, Li B, Niu L (2016) *ACS Nano* 10:5212
21. Li Z, Smeu M, Afsari S, Xing Y, Ratner MA, Borguet E (2014) *Angew Chem Int Ed* 53:1098
22. Huang C, Chen S, Baruel Ornso K, Reber D, Baghernejad M, Fu Y, Wandlowski T, Decurtins S, Hong W, Thygesen KS, Liu SX (2015) *Angew Chem Int Ed* 54:14304
23. Zhang JL, Zhong JQ, Lin JD, Hu WP, Wu K, Xu GQ, Wee AT, Chen W (2015) *Chem Soc Rev* 44:2998
24. Tao NJ (2006) *Nat Nano* 1:173
25. Xiang D, Jeong H, Lee T, Mayer D (2013) *Adv Mater* 25:4845

26. Iijima S (1991) *Nature* 354:56
27. Novoselov KS, Geim AK, Morozov SV, Jiang D, Zhang Y, Dubonos SV, Grigorieva IV, Firsov AA (2004) *Science* 306:666
28. Thompson SE, Parthasarathy S (2006) *Mater Today* 9:20
29. Ajayan PM, Ebbesen TW (1997) *Rep Prog Phys* 60:1025
30. Tans SJ, Verschueren ARM, Dekker C (1998) *Nature* 393:49
31. Dai H (2002) *Acc Chem Res* 35:1035
32. Robertson J (2007) *Mater Today* 10:36
33. Feldman AK, Steigerwald ML, Guo X, Nuckolls C (2008) *Acc Chem Res* 41:1731
34. Cao Y, Dong S, Liu S, He L, Gan L, Yu X, Steigerwald ML, Wu X, Liu Z, Guo X (2012) *Angew Chem Int Ed* 51:12228
35. Liu S, Guo X (2012) *NPG Asia Mater* 4:e23
36. Guo X (2013) *Adv Mater* 25:3397
37. Perrin ML, Burzuri E, van der Zant HSJ (2015) *Chem Soc Rev* 44:902
38. Jia C, Ma B, Xin N, Guo X (2015) *Acc Chem Res* 48:2565
39. Sun L, Diaz-Fernandez YA, Gschneidner TA, Westerlund F, Lara-Avila S, Moth-Poulsen K (2014) *Chem Soc Rev* 43:7378
40. Prins F, Barreiro A, Ruitenbergh JW, Seldenthuis JS, Aliaga-Alcalde N, Vandersypen LMK, van der Zant HSJ (2011) *Nano Lett* 11:4607
41. Guo X, Small JP, Klare JE, Wang Y, Purewal MS, Tam IW, Hong BH, Caldwell R, Huang L, O'Brien S, Yan J, Breslow R, Wind SJ, Hone J, Kim P, Nuckolls C (2006) *Science* 311:356
42. Liu S, Zhang X, Luo W, Wang Z, Guo X, Steigerwald ML, Fang X (2011) *Angew Chem Int Ed* 50:2496
43. Wang H, Muren NB, Ordinario D, Gorodetsky AA, Barton JK, Nuckolls C (2012) *Chem Sci* 3:62
44. Cao Y, Dong S, Liu S, Liu Z, Guo X (2013) *Angew Chem Int Ed* 52:3906
45. Whalley AC, Steigerwald ML, Guo X, Nuckolls C (2007) *J Am Chem Soc* 129:12590
46. Gao L, Li LL, Wang X, Wu P, Cao Y, Liang B, Li X, Lin Y, Lu Y, Guo X (2015) *Chem Sci* 6:2469
47. Darwish N, Aragones AC, Darwish T, Ciampi S, Diez-Perez I (2014) *Nano Lett* 14:7064
48. Jia C, Wang J, Yao C, Cao Y, Zhong Y, Liu Z, Liu Z, Guo X (2013) *Angew Chem Int Ed* 52:8666
49. Jia C, Migliore A, Xin N, Huang S, Wang J, Yang Q, Wang S, Chen H, Wang D, Feng B, Liu Z, Zhang G, Qu D-H, Tian H, Ratner MA, Xu HQ, Nitzan A, Guo X (2016) *Science* 352:1443
50. Quek SY, Kamenetska M, Steigerwald ML, Choi HJ, Louie SG, Hybertsen MS, Neaton JB, Venkataraman L (2009) *Nat Nano* 4:230
51. Su TA, Li H, Steigerwald ML, Venkataraman L, Nuckolls C (2015) *Nat Chem* 7:215
52. Baghernejad M, Zhao X, Baruel Orsno K, Fuego M, Moreno-Garcia P, Rudnev AV, Kaliginedi V, Vesztegom S, Huang C, Hong W, Broekmann P, Wandlowski T, Thygesen KS, Bryce MR (2014) *J Am Chem Soc* 136:17922
53. Kiguchi M, Ohto T, Fujii S, Sugiyasu K, Nakajima S, Takeuchi M, Nakamura H (2014) *J Am Chem Soc* 136:7327
54. Li L, Lo WY, Cai Z, Zhang N, Yu L (2016) *Chem Sci* 7:3137
55. Sorgenfrei S, Chiu C-Y, Gonzalez RL, Yu Y-J, Kim P, Nuckolls C, Shepard KL (2011) *Nat Nano* 6:126
56. Choi Y, Moody IS, Sims PC, Hunt SR, Corso BL, Perez I, Weiss GA, Collins PG (2012) *Science* 335:319
57. Liu S, Clever GH, Takezawa Y, Kaneko M, Tanaka K, Guo X, Shionoya M (2011) *Angew Chem Int Ed* 50:8886
58. Guo S, Artés JM, Díez-Pérez I (2013) *Electrochim Acta* 110:741
59. Osorio HM, Catarelli S, Cea P, Gluyas JB, Hartl F, Higgins SJ, Leary E, Low PJ, Martin S, Nichols RJ, Tory J, Ulstrup J, Vezzoli A, Milan DC, Zeng Q (2015) *J Am Chem Soc* 137:14319
60. Kay NJ, Higgins SJ, Jeppesen JO, Leary E, Lycoops J, Ulstrup J, Nichols RJ (2012) *J Am Chem Soc* 134:16817
61. Chen F, He J, Nuckolls C, Roberts T, Klare JE, Lindsay S (2005) *Nano Lett* 5:503
62. Xu BQ, Li XL, Xiao XY, Sakaguchi H, Tao NJ (2005) *Nano Lett* 5:1491
63. Xiao X, Nagahara LA, Rawlett AM, Tao N (2005) *J Am Chem Soc* 127:9235
64. He J, Fu Q, Lindsay S, Cizek JW, Tour JM (2006) *J Am Chem Soc* 128:14828
65. Xiao X, Brune D, He J, Lindsay S, Gorman CB, Tao N (2006) *Chem Phys* 326:138
66. Darwish N, Díez-Pérez I, Guo S, Tao N, Gooding JJ, Paddon-Row MN (2012) *J Phys Chem C* 116:21093

67. Darwish N, Diez-Perez I, Da Silva P, Tao N, Gooding JJ, Paddon-Row MN (2012) *Angew Chem Int Ed* 51:3203
68. Xu, Xiao, Yang X, Zang L, Tao (2005) *J Am Chem Soc* 127:2386
69. Li, Hihath J, Chen F, Masuda T, Zang L, Tao (2007) *J Am Chem Soc* 129:11535
70. Li Z, Li H, Chen S, Froehlich T, Yi C, Schonenberger C, Calame M, Decurtins S, Liu SX, Borguet E (2014) *J Am Chem Soc* 136:8867
71. Diez-Pérez I, Li Z, Guo S, Madden C, Huang H, Che Y, Yang X, Zang L, Tao N (2012) *ACS Nano* 6:7044
72. Pia EAD, Chi Q, Jones DD, Macdonald JE, Ulstrup J, Elliott M (2011) *Nano Lett* 11:176
73. Albrecht T, Guckian A, Kuznetsov AM, Vos JG, Ulstrup J (2006) *J Am Chem Soc* 128:17132
74. Capozzi B, Chen Q, Darancet P, Kotiuga M, Buzzeo M, Neaton JB, Nuckolls C, Venkataraman L (2014) *Nano Lett* 14:1400
75. Rocha AR, Garcia-suarez VM, Bailey SW, Lambert CJ, Ferrer J, Sanvito S (2005) *Nat Mater* 4:335
76. Hayakawa R, Karimi MA, Wolf J, Huhn T, Zollner MS, Herrmann C, Scheer E (2016) *Nano Lett* 16:4960
77. Frisenda R, Harzmann GD, Celis Gil JA, Thijssen JM, Mayor M, van der Zant HS (2016) *Nano Lett* 16:4733
78. Wagner S, Kisslinger F, Ballmann S, Schramm F, Chandrasekar R, Bodenstern T, Fuhr O, Secker D, Fink K, Ruben M, Weber HB (2013) *Nat Nano* 8:575
79. Aragonés AC, Aravena D, Cerda JI, Acis-Castillo Z, Li H, Real JA, Sanz F, Hihath J, Ruiz E, Diez-Perez I (2016) *Nano Lett* 16:218
80. Brooke RJ, Jin C, Szumski DS, Nichols RJ, Mao BW, Thygesen KS, Schwarzacher W (2015) *Nano Lett* 15:275
81. Meded V, Bagrets A, Arnold A, Evers F (2009) *Small* 5:2218
82. Lewis PA, Inman CE, Yao Y, Tour JM, Hutchison JE, Weiss PS (2004) *J Am Chem Soc* 126:12214
83. Blum AS, Kushmerick JG, Long DP, Patterson CH, Yang JC, Henderson JC, Yao Y, Tour JM, Shashidhar R, Ratna BR (2005) *Nat Mater* 4:167
84. Meng F, Hervault YM, Shao Q, Hu B, Norel L, Rigaut S, Chen X (2014) *Nat Commun* 5:3023
85. Meng F, Hervault Y-M, Norel L, Costuas K, Van Dyck C, Geskin V, Cornil J, Hng HH, Rigaut S, Chen X (2012) *Chem Sci* 3:3113
86. Wesenhagen P, Areephong J, Fernandez Landaluce T, Heureux N, Katsonis N, Hjelm J, Rudolf P, Browne WR, Feringa BL (2008) *Langmuir* 24:6334
87. Logtenberg H, van der Velde JHM, de Mendoza P, Areephong J, Hjelm J, Feringa BL, Browne WR (2012) *J Phys Chem C* 116:24136
88. van der Molen SJ, Liao J, Kudernac T, Agustsson JS, Bernard L, Calame M, van Wees BJ, Feringa BL, Schönenberger C (2009) *Nano Lett* 9:76
89. van Leeuwen T, Pijper TC, Areephong J, Feringa BL, Browne WR, Katsonis N (2011) *J Mater Chem* 21:3142
90. Arramel, Pijper TC, Kudernac T, Katsonis N, van der Maas M, Feringa BL, van Wees BJ (2013) *Nanoscale* 5:9277
91. Van Herpt JT, Areephong J, Stuart MCA, Browne WR, Feringa BL (2014) *Chem Eur J* 20:1737
92. Guo X, Myers M, Xiao S, Lefenfeld M, Steiner R, Tulevski GS, Tang J, Baumert J, Leibfarth F, Yardley JT, Steigerwald ML, Kim P, Nuckolls C (2006) *Proc Natl Acad Sci USA* 103:11452
93. Liu S, Wei Z, Cao Y, Gan L, Wang Z, Xu W, Guo X, Zhu D (2011) *Chem Sci* 2:796
94. Cao Y, Liu S, Shen Q, Yan K, Li P, Xu J, Yu D, Steigerwald ML, Nuckolls C, Liu Z, Guo X (2009) *Adv Funct Mater* 19:2743
95. Cao Y, Wei Z, Liu S, Gan L, Guo X, Xu W, Steigerwald ML, Liu Z, Zhu D (2010) *Angew Chem Int Ed* 49:6319
96. Kim D, Jeong H, Lee H, Hwang WT, Wolf J, Scheer E, Huhn T, Jeong H, Lee T (2014) *Adv Mater* 26:3968
97. Seo S, Min M, Lee SM, Lee H (2013) *Nat Commun* 4:1920
98. Guo X, Xiao S, Myers M, Miao Q, Steigerwald ML, Nuckolls C (2009) *Proc Natl Acad Sci USA* 106:691